

Propagation characteristics of longitudinal-torsion coupled waves in phononic crystal rods of chiral materials

P. DAI, R. WANG

Tianjin University, Tianjin 300054, China, e-mail: daipengshuai666@163.com

THE CHIRAL PROPERTIES OF CHIRAL MATERIALS have a great influence on the wave propagation. Applying chiral materials to the design of phononic crystal rods not only increases the design space, but also may have other potential advantages. There is a lack of research on designing phononic crystal rods using chiral materials and the propagation characteristics of elastic waves in phononic crystal rods made of chiral materials. In this study, chiral materials are introduced into the design of phonon crystal rods for the first time, Bragg scattering type and local resonance type phononic crystal rods are designed using chiral materials. Dispersion equations for the propagation of longitudinal-torsion coupled waves in the phononic crystal rods are derived, and the effect of the chirality of the materials on their bandgap range is studied. The study shows that: in Bragg scattering type phonon crystal rods, material chirality can greatly affect the bandgap, among them, the chiral direction has the greatest effect, and in order to obtain a low-frequency wide bandgap, the chiral coefficients of the materials should be increased as much as possible with the chiral directions of the two cells being opposite; in the local resonance type phonon crystal rod, only two types of oscillators are added to the material simultaneously to produce a band gap, and the starting frequency obtained is much lower than that of the Bragg scattering type.

Key words: chiral material, band gap, phononic crystal rods, longitudinal-torsion waves.



Copyright © 2023 The Authors.

Published by IPPT PAN. This is an open access article under the Creative Commons Attribution License CC BY 4.0 (<https://creativecommons.org/licenses/by/4.0/>).

1. Introduction

ROD STRUCTURES ARE WIDELY USED IN EVERYDAY LIFE, along with engineering applications such as aerospace, ship building, and civil engineering. Vibrations are inevitable in engineering structures, which necessitates research into the dynamics and vibration reduction design of beam and rod structures [1, 2]. The band gap properties of phonon crystals provide novel ideas for vibration isolation and noise reduction in engineering structures [3].

The generation of bandgap in phononic crystals is mainly based on two mechanisms: one is that Bragg scattering occurs between neighboring lattices during wave propagation and leads to the continuous dispersion of energy, and the resulting bandgap is called the Bragg bandgap [4]; the other is that the energy of

the wave is absorbed by the local resonance cells or structures in the phononic crystals in the process of wave propagation to the extent that it cannot propagate forward, and the resulting bandgap is called the local resonance bandgap [5]. Among them, the bandgap range of the former has a strong relationship with the lattice size of the crystal, and generally can only suppress waves with wavelengths smaller than or equal to its lattice size, and it is not easy to generate a bandgap at low frequencies [4]; the bandgap range of the local resonance-type phononic crystals is dependent on the intrinsic frequency of the resonance cell, which is free from the control of the lattice size within the bandgap range, and is conducive to the realization of the low-frequency bandgap, but the bandgap range of this type of phononic crystal is generally narrower. Therefore, realizing both low frequency and wide bandgap by using a small and simple structure has been one of the hot issues in the field of phononic crystals.

Studies have shown that phononic crystal beams, rods, plates, and other structures can also generate bandgap [6–8]. In engineering, phonon crystals can be used to make custom structures for controlling elastic waves. LI *et al.* [9] demonstrated variable-section phononic crystal beams; JIANG *et al.* [10] and WANG *et al.* [11] worked with folded piezoelectric phononic crystal beams and phononic crystal tracks with good vibration isolation effects. The microstructural characteristic lengths of the materials used in these structures are considerably smaller than the elastic wave wavelengths, presented in contemporary studies; thus, the effect of microstructure can be neglected [12].

In recent years, with the development of micro- and nano-phonon crystals, materials with microstructural features of length comparable to their wavelengths have gradually attracted attention. Researchers are focusing on studying the propagation properties of elastic waves in them and using them to make phonon crystals and phonon crystal structures. When the wavelength of elastic waves is comparable to the characteristic length of the microstructure, the microstructure of the material considerably influences the elastic waves [13–16]. Therefore, the band gap properties of such phononic crystals can be modulated by tuning their microstructure parameters to provide more design space for designing phononic crystals and phononic crystal structures [12]. MIAO *et al.* [17] used micropolar materials to reverse the design of phononic crystal beams, which can modulate the size effect to modulate the band gap of phononic crystals, considerably improving their design range. Similar to micropolar materials, chiral materials have chiral microstructures [18]. When the characteristic size is comparable to the material wavelength, the chiral characteristics of chiral materials also considerably affect wave propagation [19].

Chirality is a geometric property, which an object cannot coincide with its mirror image after operations such as translation and rotation. Because of these unique geometric properties, chiral structures have coupled deformation prop-

erties such as stretch-twist and bend-twist [20], as a result, when elastic waves propagate in chiral materials, the motion of particles takes the form of coupled motion of macroscopic advection and microscopic micro-rotation. These coupled motions affect the scattering and dispersion behavior of elastic waves as they propagate [19, 21–23], enhancing the control of elastic waves by chiral materials. LAKHTAKIA [23] demonstrated that chiral parameters can affect the scattering and dispersion of elastic waves, and the total reflection of elastic waves can be achieved by appropriately adjusting the chiral parameters of chiral materials. YANG *et al.* [21] showed that reducible reflected plane waves can be excited using chiral materials, which can be used as anechoic coatings. Several contemporary studies on chiral structures have shown that because of their unique geometry, large in-plane deformability, porosity, and other characteristics, chiral structures have advantages such as excellent local wave capability and strong energy dissipation ability [24, 25]. Theoretically, chiral materials also have these advantages because of their chiral microstructures. Therefore, designing phononic crystal rods using chiral materials can increase the space of designs and may have other potential advantages. Contemporary research lacks information regarding the design of phononic crystal rods using chiral materials as well as the propagation characteristics of elastic waves in phononic crystal rods made of chiral materials.

In this study, we introduced chiral materials into the design of phononic crystal rods for the first time and two types of phonon crystal rods are designed using chiral materials. One is a phonon crystal rod comprising different chiral materials, that is, the Bragg scattering type phonon crystal rod, and the other is a local resonance type phonon crystal rod equipped with oscillators. Then, the wave equations for longitudinal torsional coupling propagation and their dispersion relations are derived, and the effect of material chirality on their bandgap ranges is studied.

2. Mechanical model

A slender rod of a phonon crystal comprising chiral material is examined in this study (Fig. 1). The phonon crystal unit comprised two cells, each of which is a slender rod cell with a circular cross-section, and each cell comprised a transversely isotropic chiral material with chirality only in the axial direction and isotropic in the other directions. The lengths of the two cells are a_1 and a_2 ,



FIG. 1. Schematic diagram of phonon crystal rod of chiral material.

and the cell-to-cell contact is perfect, which satisfied the condition of a continuous interface. The propagation characteristics of the longitudinal-torsion coupled waves along the axis direction are studied.

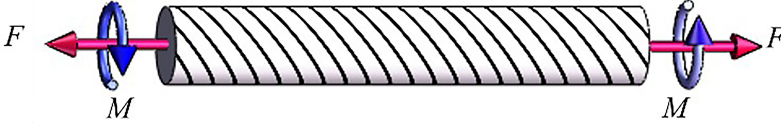


FIG. 2. Chiral material slender rod force diagram.

First, the constitutive relation for the tensile-torsion of a chiral slender rod is derived. For a chiral material slender rod, as shown in Fig. 2 F is the axial force of the rod, M is the torque of the rod u is axial displacement, ϕ is axial torsion.

According to [2], the strain energy of the chiral slender rod is calculated using

$$(2.1) \quad U = \int_0^L \frac{1}{2} A \varepsilon^2 + \frac{1}{2} C \kappa^2 + B \varepsilon \kappa dz,$$

where ε , κ , L , A , C , B and z are the axial strain, axial torque, rod length, tensile stiffness, torsional stiffness, coupling stiffness, and axial coordinate, respectively.

The virtual work done by the axial force F and the torque M is calculated using

$$(2.2) \quad \delta W = F \delta u + M \delta \phi.$$

From the geometric relationship and the definition of strain, we obtain

$$(2.3) \quad \delta u = \varepsilon L, \quad \delta \phi = \kappa L, \quad \varepsilon = \frac{\partial u}{\partial z}, \quad \kappa = \frac{\partial \phi}{\partial z}.$$

According to the variation of strain energy and the functional reciprocity theorem we obtain

$$(2.4) \quad \delta W - \delta U = 0.$$

Then, the constitutive relation of the chiral slender rod can be obtained by

$$(2.5) \quad F = A \frac{\partial u}{\partial z} + B \frac{\partial \phi}{\partial z}, \quad M = C \frac{\partial \phi}{\partial z} + B \frac{\partial u}{\partial z}.$$

The relationship between A , B , and C is given using

$$(2.6) \quad B = \pm \sqrt{c_h AC},$$

where c_h is the chiral coefficient; c_h represents the degree of stretch-torsion coupling. A larger chiral coefficient implies stretch-induced larger torsion. The chiral direction can be positive and negative when B is positive and negative, respectively, indicating the difference in the direction of stretch-induced torsion [26].

3. Problem solving

The wave equation (3.1) is obtained by replacing the axial force and torque in the constitutive equation (2.5) with the inertial force and moment of inertia,

$$(3.1) \quad \begin{aligned} A \frac{\partial^2 u}{\partial z^2} + B \frac{\partial^2 \phi}{\partial z^2} &= \rho A_p \frac{\partial^2 u}{\partial t^2}, \\ C \frac{\partial^2 \phi}{\partial z^2} + B \frac{\partial^2 u}{\partial z^2} &= \rho J_p \frac{\partial^2 \phi}{\partial t^2}, \end{aligned}$$

where A_p , J_p , and ρ are the area of the cross-section, moment of inertia of the cross-section, material density and t is the time.

The general solution of displacement and torsion is expressed using:

$$(3.2) \quad \begin{aligned} u &= A_1 e^{ik_1 z - i\omega t} + A_2 e^{ik_2 z - i\omega t} + B_1 e^{ik_1 z - i\omega t} + B_2 e^{ik_2 z - i\omega t}, \\ \phi &= Q_1 A_1 e^{ik_1 z - i\omega t} + Q_2 A_2 e^{ik_2 z - i\omega t} + Q_3 B_1 e^{ik_1 z - i\omega t} + Q_4 B_2 e^{ik_2 z - i\omega t}. \end{aligned}$$

The solution procedure is presented in Appendix Q_1 – Q_4 and k_1 – k_4 can be found in Appendix, A_1 , A_2 , B_1 , and B_2 are arbitrary constants, and ω is the angular frequency.

By presenting Eq. (3.2) in matrix form, we can obtain

$$(3.3) \quad \begin{bmatrix} u \\ \phi \end{bmatrix} = \begin{bmatrix} D_1 & D_2 & D_3 & D_4 \\ D_5 & D_6 & D_7 & D_8 \end{bmatrix} G,$$

where $G = [A_1 \ A_2 \ B_1 \ B_2]$ are arbitrary constant matrix, D_1 – D_8 are the elements before the coefficients of the general solution of Eq. (3.1).

By combining Eqs. (2.5) and (3.3), we can obtain

$$(3.4) \quad \begin{bmatrix} F \\ M \end{bmatrix} = \begin{bmatrix} D_9 & D_{10} & D_{11} & D_{12} \\ D_{13} & D_{14} & D_{15} & D_{16} \end{bmatrix} G,$$

where D_9 – D_{16} are the elements obtained by inserting Eq. (3.2) in Eq. (2.5). Appendix presents the method for obtaining the values of D_1 – D_{16} .

After obtaining Eqs. (3.3) and (3.4), $z = 0$ is used to obtain the displacement, torsions, axial forces, and torque on the left side of a cell; these are represented in matrix form to obtain

$$(3.5) \quad [u^L \ \phi^L \ F^L \ M^L]^T = D^L G,$$

where elements D^L are the value of D in Eqs. (3.2) and (3.3) at $z = 0$ and the superscript “ L ” denotes the left side.

$z = a_1$ is used to obtain the displacement, torsion, axial force, and torque on the right side of this cell and represented in matrix form to obtain

$$(3.6) \quad [u^R \ \phi^R \ F^R \ M^R]^T = D^R G.$$

The elements D^R are the value of D in Eqs. (3.2) and (3.3) at $z = a_1$, and the superscript “ R ” denotes the right side.

When Eqs. (3.4) and (3.5) are combined and the same part is eliminated, the transfer matrix of this cell can be obtained, which is

$$(3.7) \quad T_1 = D^R(D^L)^{-1}.$$

Similarly, the transfer matrix of the other cell is obtained as T_2 . The two cells are in perfect contact; therefore, the transfer matrix of the whole unit is obtained by multiplying the two transfer matrices as

$$(3.8) \quad T = T_1 T_2.$$

The dispersion equation (3.8) is obtained according to the Bloch boundary condition [29],

$$(3.9) \quad \det(T - e^{ika} I) = 0,$$

where $a = a_1 + a_2$, k is the number, and I is the unit matrix.

Next, the locally resonant phonon crystal rod is discussed. First, torsionally moving ring oscillators are added. As shown in Fig. 3, ring oscillators are added to the right side of each cell, and each oscillator comprised a torque spring with a negligible mass and a circular mass block.

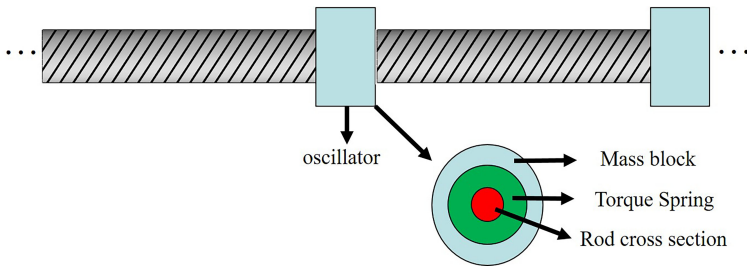


FIG. 3. Schematic diagram of phonon crystal rod with added torsion oscillators.

The torsion φ^n of the n th cell annular oscillator is assumed to be given using

$$(3.10) \quad \varphi^n = V^n e^{i\omega t},$$

where φ^n is the torsion of the n th cell annular oscillator, V^n is the amplification, and ω is the angular frequency.

Then, by analyzing the force on the oscillator, the equation of motion of the oscillator is obtained as

$$(3.11) \quad I_p \frac{\partial^2 \varphi^n}{\partial t^2} = M_P,$$

where

$$(3.12) \quad M_P = K_h(\varphi^n - \phi^R),$$

as the torque transmitted on the torque spring, and ϕ^R , K_h , I_P are torsion on the right side of the n th cell, equivalent stiffness of the torque spring, and moment of inertia of the oscillator mass, respectively.

Equations (3.9)–(3.11) are used to express φ^n by ϕ^R for

$$(3.13) \quad \varphi^n = \phi^R \left(\frac{K_h}{K_h + I_P \omega^2} \right).$$

Then, the moment on the right side of the cell is

$$(3.14) \quad M^{RN} = M^R + M_P.$$

M^R in Eq. (3.5) is replaced with M^{RN} , and the elements in D^R are changed and inserted in Eq. (3.6). Then, the transfer matrix T_1^1 with the torsional oscillator is obtained and the dispersion relation is given using

$$(3.15) \quad \det(T_1^1 - e^{ika_1}) = 0.$$

Next, resonant phonon crystal rods with longitudinally moving oscillators are added, as shown in Fig. 4, to the right side of each cell. Each oscillator comprised a spring of negligible mass and a mass block.

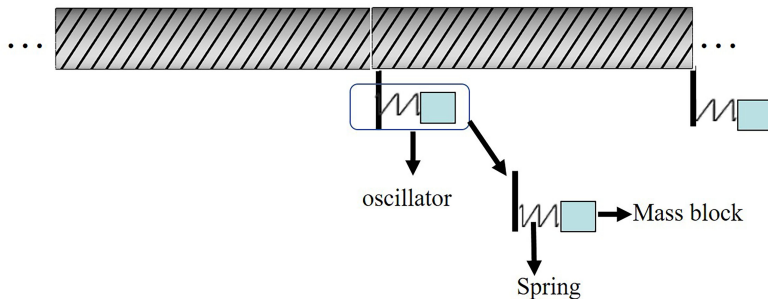


FIG. 4. Schematic diagram of phonon crystal rod with added longitudinal oscillators.

Using the similar process of obtaining Eq. (3.14) and replacing φ^n and ϕ^R with the displacements of the longitudinal oscillators and the displacement on the right side of the n th cell, the force F^{RN} on the right side of the cell with the addition of the longitudinal oscillator can be obtained. Then, the dispersion relation can be obtained by using a method similar to that described above for adding a torsional oscillator. Only here F^R is replaced by F^{RN} . If $F^R \cdot M^R$ are replaced then the dispersion relation can be obtained with both oscillators added.

4. Numerical results and discussion

4.1. Result comparison

When the chiral coefficient in this study is approximately zero, longitudinal and torsional waves can be approximately decoupled and the band structure of torsional and longitudinal waves can be degraded from Eq. (3.8). The degradation result should be the same as the band structure of the longitudinal and torsional waves of the phonon crystal rod with the same material parameters. In order to verify the correctness of this work, the band structure of the longitudinal wave is degenerated and compared with that of the phononic crystal rod made of Frazier elastic material using the parameters from Frazier's paper [28], and the results are shown in Fig. 5. From Fig. 5, it can be seen that our degenerate results are in general agreement with those in the literature, proving, the correctness of our method.

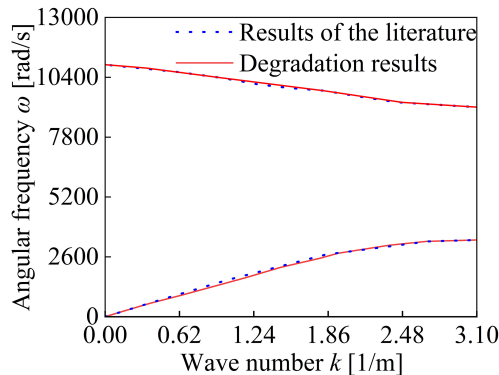


FIG. 5. Comparison chart of the results.

Then, the propagation of longitudinal-torsion coupled waves in phonon crystal rods is numerically studied and discussed. Most biological materials, such as wood and bone, are chiral materials. For example, cartilage tissue, has elastic and shear moduli of 0.1–1 GPa and 0.01–0.1 GPa, respectively [29]. In this section,

the moduli of elasticity and shear are set to 0.2 GPa and 0.01 GPa, respectively. The modulus of elasticity multiplied by the area is the tensile stiffness, A , and the shear modulus multiplied by the extreme moment of inertia is the torsional stiffness C . The cross-sectional radius of the slender rod and density ρ are set to 0.05 m and 1012 kg/m³, respectively. The length a is 2 m, and the lengths of two cells a_1 and a_2 are 1 m each.

4.2. Bragg scattering type phonon crystal rod

4.2.1. The same chiral direction of cell. The performance parameters of material chirality of chiral material rod cell are the chiral coefficient magnitude and the chiral direction. Next, from these two aspects, the influence of material chirality is investigated. According to the dispersion equation (3.9), the energy band structure of the phononic crystal rods is obtained. The chiral direction of both cells is considered to be positive, i.e., B takes both positive values. The chiral coefficient of c_h is considered between 0 and 1. Therefore, the chiral coefficients of the two cells are $c_h = 0.1$ and $c_h = 0.5$, respectively, as shown in Fig. 6(a), where the pink part represents the band gap. Thereafter, the chiral coefficient of one cell is set to $c_h = 0.1$, and the chiral coefficient of the other cell gradually increases to obtain the curve of the first band gap range with different chiral coefficient differences, as shown in Fig. 6(b). The starting frequency is the frequency at which the bandgap begins, the lower edge of the bandgap in Fig. 6(a), the cut-off frequency is the frequency at which the bandgap ends the upper edge of the bandgap in Fig. 6(a), and the difference between the cut-off frequency and the starting frequency is the width of the bandgap.

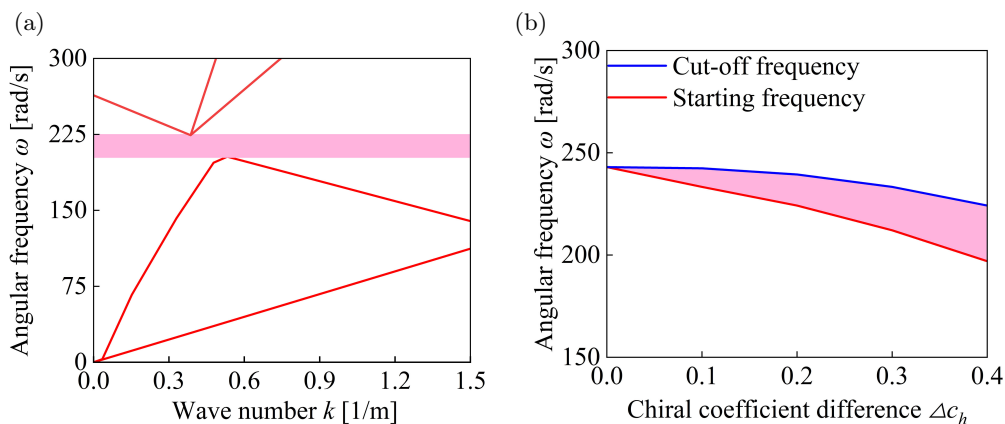


FIG. 6. Energy band structures of two cells with different chiral coefficients and the effect of different chiral coefficients on the first band gap: (a) energy band structure and (b) change of band gap with different chiral coefficient differences Δc_h .

As shown in Fig. 6, the different material chiral coefficient of the two cells can open the band gap of the phonon crystal rods. Thus, the chirality of the material can influence the propagation of elastic waves of the phonon crystal structures. As the differences in the chiral coefficient increased, the first band gap range gradually increased, and the starting frequency and cutoff frequency both decreased. The increase in the chiral coefficient difference can make the difference in the material properties of the two cells larger, making the band gap wider which is easy to understand.

The decrease of the starting frequency and cutoff frequency may be caused by the increase of the chiral coefficient. In order to prove this point. Controlling the difference of the chiral coefficient constant, taken as $\Delta c_h = 0.1$, the curve of the variation of the first band gap with a smaller chiral cell is made, as shown in Fig. 7(a). Controlling the difference of the chiral coefficient constant, taken as $\Delta c_h = 0.15$, the curve of the variation of the first band gap with a small chiral cell is made, as shown in Fig. 7(b).

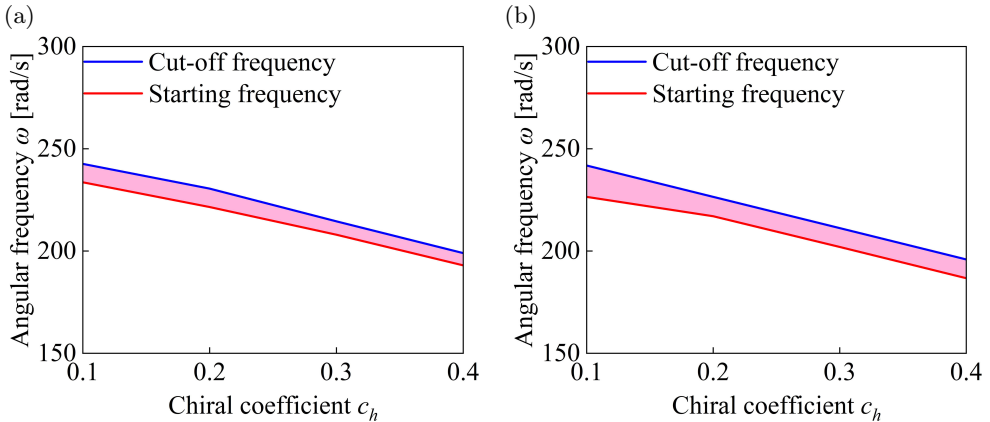


FIG. 7. Effect of chiral coefficients on band gap range when the difference in chiral coefficients is constant: (a) $\Delta c_h = 0.1$ and (b) $\Delta c_h = 0.15$.

From Fig. 7, it can be seen that the starting and cut-off frequencies of the first band gap decrease with the increase of the chiral coefficient at a constant difference of the chiral coefficients of the two cells, and the band gap width decreases slightly but not significantly. This can indicate that the chirality of the material is favorable for the phonon crystal rod to open the band gap at low frequencies, and the chiral coefficient of the material should be increased as much as possible if we want to achieve the control of low frequency waves.

4.2.2. Opposite direction of cell chirality. The chiral direction of one cell is assumed to be positive and the other is considered negative. That is, one cell of

B is positive, and for the other cell, B is negative. First, for the two cells, chiral coefficients are set to $c_h = 0.5$ for obtaining the energy band structures, as shown in Fig. 8(a), where the pink part represents the band gap. Then, the chiral coefficients of the two cells gradually increase to obtain curves of the first band gap range with the different chiral coefficients, as shown in Fig. 8(b).

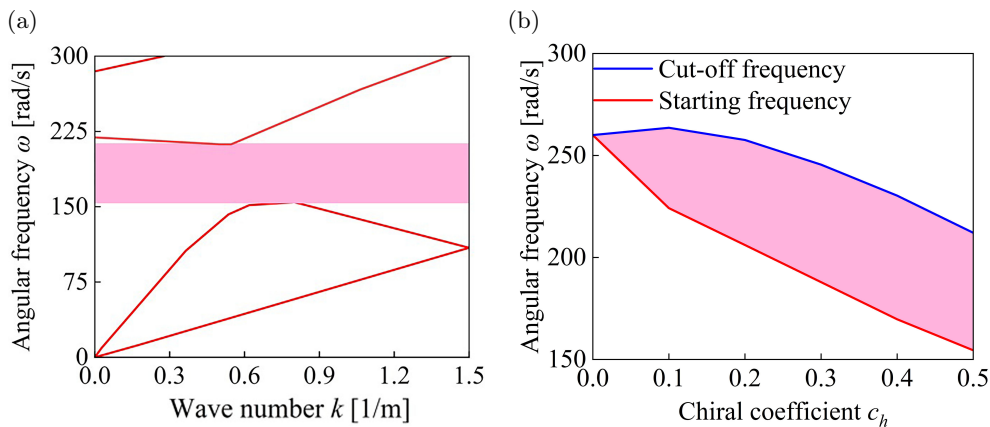


FIG. 8. Energy band structure of two cells with opposite chiral directions and the effect of chiral coefficients on the first band gap: (a) energy band structure and (b) variation of band gap with chiral coefficients c_h .

As shown in Fig. 8, the different chiral directions of the two cells can also open the band gap of the phonon crystal rod, and the band gap range is wider and the starting frequency is lower than that in Fig. 6. The chiral direction of the material represents the direction of twisting produced when the chiral rod is stretched. The opposite chiral direction produces the opposite torsion when the chiral rod vibrates in the longitudinal direction. Obviously, in this case, the difference in material properties between the cells is greater, so that a wider band gap is produced. Also, similar to above, an increase in the material chiral coefficient still resulted in lower starting and cutoff frequencies. The aim behind designing the phononic crystal rod is to obtain a wide band gap at low frequencies. Considering opposite chiral directions for the two cells is more favorable for achieving this goal.

4.3. Local resonant phonon crystal rods

According to some literature [3] the equivalent stiffness of the selectable spring is that the stiffness of the torque spring K_h is 4 kN, and the stiffness of the spring K_t is 100 kN/m. The oscillator is selected as a denser lead with a density of 11 600 kg/m³. The diameters of the inner and outer ring oscilla-

tors are set to 0.14 m and 0.16 m, respectively; thus, the rotational inertia I_p of the oscillator is obtained. The longitudinal oscillator is taken as a square with a length of 0.1 m, and it is used to obtain its mass m_p .

The tensile and torsional stiffnesses of the chiral material are the same as above, with a cell length of 1 m and a chiral coefficient of $c_h = 0.5$. The energy band structure without oscillator, with only torsional oscillator, with only longitudinal motion oscillator, and with both oscillators is shown in Fig. 9(a)–(d), respectively.

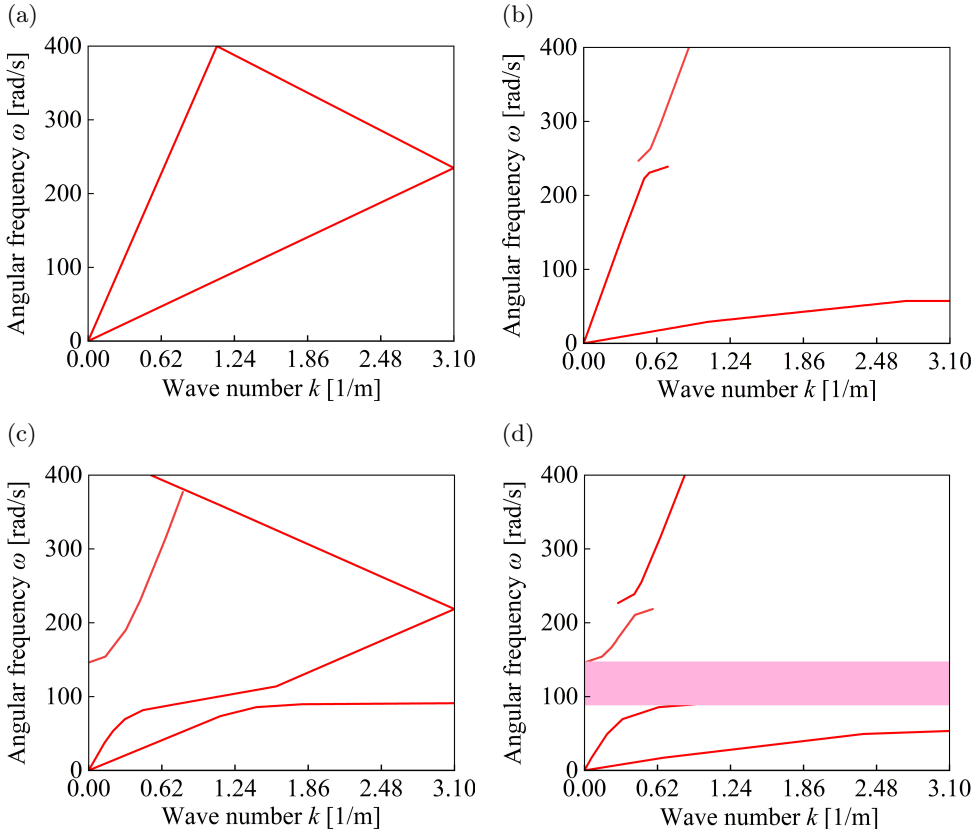


FIG. 9. Energy band structure of resonant phonon crystal: (a) without oscillator, (b) with torsional oscillator, (c) with longitudinal vibrational oscillator, and (d) with both oscillators.

As shown in Fig. 9, the band gap is not generated by the phononic crystal rod when no oscillators are added or in case of only one type of oscillator; the band gap is opened only when two types of oscillators are added. The starting frequency of this band gap is much lower than that of the Bragg scattering phononic crystal rod, which is consistent with the conclusion that resonant phononic crys-

tals are more likely to produce a low-frequency band gap. Moreover, as shown in Fig. 9(b) and (c), simply adding one type of oscillator cannot produce a band gap, but the addition of one type of oscillator can affect the energy band structure, and different combinations of oscillators have different effects on the energy band structures.

5. Conclusion

In this study, chiral materials are introduced into the design of phonon crystal rods for the first time, the Bragg scattering type and local resonance type phononic crystal rods are designed using chiral materials, and the propagation characteristics of longitudinal-torsional coupled waves in them are studied. In Bragg scattering type phonon crystal rods, the band gap is generated because of the differences in chiral coefficients and chiral directions, with the chiral direction having a greater effect. An increase in the chiral coefficient of the material can decrease the starting and cutoff frequencies of the phonon crystal rods. And the widest band gap range can be obtained when the material chirality is in the opposite direction. Therefore, in order to obtain a low-frequency wide bandgap, the chiral coefficient of the material should be increased as much as possible with the chiral directions of the two cells being opposite. In the local resonance type phonon crystal rod, adding only one type of oscillator affected the energy band structure but did not produce a band gap. Only two types of oscillators are added to the material simultaneously to produce a band gap, and the starting frequency obtained is much lower than that of the Bragg scattering type. These findings will provide the theoretical basis for the design of phononic crystal structures and vibration isolation structures.

Appendix

The solution of the wave equation (3.1) is shown here. First, the solution of displacement and torsion is given using [31]

$$(A.1) \quad \begin{aligned} u &= U' e^{ikz - i\omega t}, \\ \phi &= \Omega e^{ikz - i\omega t}, \end{aligned}$$

where U' and Ω are the amplitudes of longitudinal and torsional waves, respectively.

It is inserted back into the wave equation (3.1), we can obtain

$$(A.2) \quad \begin{bmatrix} -k^2 A + \rho A_p \omega^2 & -k^2 B \\ -k^2 B & -k^2 C + \rho J_p \omega^2 \end{bmatrix} \begin{bmatrix} U \\ \Omega \end{bmatrix} = 0.$$

Equation (A.3) is obtained according to the condition that the system of equations has a solution

$$(A.3) \quad \det \left(\begin{bmatrix} -k^2 A + \rho A_p \omega^2 & -k^2 B \\ -k^2 B & -k^2 C + \rho J_p \omega^2 \end{bmatrix} \right) = 0.$$

The amplitude ratio of torsion and displacement is given using:

$$(A.4) \quad Q = \frac{\Omega}{U'} = \frac{-k^2 A + \rho A_p \omega^2}{k^2 B}.$$

The four solutions of k are obtained using Eq. (A.3), and the relationship between the four solutions is given using:

$$(A.5) \quad k_1 = -k_2, \quad k_3 = -k_4.$$

The general solution of displacement and torsion is expressed using:

$$(A.6) \quad \begin{aligned} u &= A_1 e^{ik_1 z - i\omega t} + A_2 e^{ik_2 z - i\omega t} + B_1 e^{ik_1 z - i\omega t} + B_2 e^{ik_2 z - i\omega t}, \\ \phi &= Q_1 A_1 e^{ik_1 z - i\omega t} + Q_2 A_2 e^{ik_2 z - i\omega t} + Q_3 B_1 e^{ik_1 z - i\omega t} + Q_4 B_2 e^{ik_2 z - i\omega t}, \end{aligned}$$

where Q_1 – Q_4 represent the amplitude ratio obtained by inserting the corresponding k , and A_1 , A_2 , B_1 , and B_2 are arbitrary constants.

The solutions of the axial force and torque are obtained by considering the instanton equation (2.5). This is organized in matrix form as:

$$(A.7) \quad \begin{bmatrix} u \\ \phi \end{bmatrix} = \begin{bmatrix} D_1 & D_2 & D_3 & D_4 \\ D_5 & D_6 & D_7 & D_8 \end{bmatrix} \begin{bmatrix} A_1 \\ A_2 \\ B_1 \\ B_2 \end{bmatrix},$$

$$(A.8) \quad \begin{bmatrix} F \\ M \end{bmatrix} = \begin{bmatrix} D_9 & D_{10} & D_{11} & D_{12} \\ D_{13} & D_{14} & D_{15} & D_{16} \end{bmatrix} \begin{bmatrix} A_1 \\ A_2 \\ B_1 \\ B_2 \end{bmatrix},$$

where D_1 – D_8 denote the elements corresponding to the coefficients preceding the general solution, and D_9 – D_{16} are the elements obtained by inserting Eq. (3.3) in Eq. (2.5).

References

1. D.M. MEAD, *Wave propagation in continuous periodic structures: research contributions from Southampton, 1964–1995*, Journal of Sound and Vibration, **190**, 495–524, 1996.
2. D. RICHARDS, D.J. PINES, *Passive reduction of gear mesh vibration using a periodic drive shaft*, Journal of Sound and Vibration, **264**, 317–342, 2003.

3. M. OUDICH, N.J. GERARD, Y. DENG, Y. JING, *Tailoring structure-borne sound through bandgap engineering in phononic crystals and metamaterials: a comprehensive review*, *Advanced Functional Materials*, **33**, 2206309, 2023.
4. X. WEN, J. WEN, D. YU, G. WANG, Y. LIU, X. HAN, *Phonon Crystals*, Defense Industry Press, Beijing, 2009.
5. Z. LIU, X. ZHANG, Y. MAO, Y.Y. ZHU, Z. YANG, C.T. CHAN, P. SHENG, *Locally resonant sonic materials*, *Science*, **289**, 1734–1736, 2000.
6. Y. XIAO, J. WEN, G. WANG, X. WEN, *Theoretical and experimental study of locally resonant and bragg band gaps in flexural beams carrying periodic arrays of beam-like resonators*, *Journal of Vibration and Acoustics-Transactions of ASME*, **135**, 041006, 2013.
7. J. ZHAO, Q. WANG, X. DENG, K. CHOE, R. ZHONG, C. SHUAI, *Free vibrations of functionally graded porous rectangular plate with uniform elastic boundary conditions*, *Composites Part B: Engineering*, **168**, 106–120, 2019.
8. G. WANG, X. WEN, J. WEN, Y. LIU, *Quasi-one-dimensional periodic structure with locally resonant band gap*, *Journal of Applied Mechanics*, **73**, 167–170, 2005.
9. T. LI, X. MA, Q. ZHANG, Z. WANG, *Band gap properties of periodic tapered beam structure using traveling wave method*, *Journal of Theoretical and Applied Mechanics*, **54**, 1297–1308, 2016.
10. S. JIANG, L. DAI, H. CHEN, H. HU, W. JIANG, X. CHEN, *Folding beam-type piezoelectric phononic crystal with low-frequency and broad band gap*, *Applied Mathematics and Mechanics*, **38**, 411–422, 2017.
11. P. WANG, Q. YI, C. ZHAO, M. XING, J. TANG, *Wave propagation in periodic track structures: band-gap behaviours and formation mechanisms*, *Archive of Applied Mechanics*, **87**, 503–519, 2017.
12. Y. LI, P. WEI, Y. ZHOU, *Band gaps of elastic waves in 1-D phononic crystal with dipolar gradient elasticity*, *Acta Mechanica*, **227**, 1005–1023, 2015.
13. S.K. TOMAR, M. GARG, *Reflection and transmission of waves from a plane interface between two microstretch solid half-spaces*, *International Journal of Engineering Science*, **43**, 139–169, 2005.
14. V.R. PARFITT, A.C. ERINGEN, *Reflection of plane waves from the flat boundary of a micropolar elastic half-space*, *The Journal of the Acoustical Society of America*, **45**, 1258–1272, 2005.
15. H.G. GEORGIADIS, I. VARDOLAKIS, E.G. VELGAKI, *Dispersive Rayleigh-wave propagation in microstructured solids characterized by dipolar gradient elasticity*, *Journal of Elasticity*, **74**, 17–45, 2004.
16. R. LIANGGEGA, J. LALVOHBIKA, S.S. SINGH, *Incident waves at the surface of micropolar porous materials*, *International Journal of Computational Materials Science and Engineering*, **11**, 2250002, 2022.
17. J. LI, Z. MIAO, S. LI, Q. MA, *Inverse design of micro phononic beams incorporating size effects via tandem neural network*, *Materials*, **16**, 1518, 2023.
18. H.C. ZHAO, L.C. BIAN, T. ZHANG, G.J. TONG, P.S. DAI, *Hierarchical chirality of biofilament induced by its chiral microstructure*, *Physica Scripta*, **97**, 055002, 2022.

19. C.C. SUNG, R. RO, Y.M. CHANG, *Scattering characteristics of the chiral slab for normally incident longitudinal elastic waves*, *Wave Motion*, **30**, 135–142, 1999.
20. P. SHARMA, *Size-dependent elastic fields of embedded inclusions in isotropic chiral solids*, *International Journal of Solids and Structures*, **41**, 6317–6333, 2004.
21. S.K. YANG, S.Y. HSIA, *Chiral composites as underwater acoustic attenuators*, *IEEE Journal of Oceanic Engineering*, **25**, 139–145, 2000.
22. R.R. SUNG, *Parametric study of reflection characteristics at achiral-chiral interfaces*, *Japanese Journal of Applied Physics*, **36**, 5208–5213, 1997.
23. A. LAKHTAKIA, V.K. VARADAN, V.V. VARADAN, *Reflection of elastic plane waves at a planar achiral–chiral interface*, *The Journal of the Acoustical Society of America*, **87**, 2314–2318, 1990.
24. N. KARATHANASOPOULOS, J.F. GANGHOFFER, *Chiral and non-centrosymmetric effects on the nonlinear wave propagation characteristics of architected cellular materials*, *Waves in Random and Complex Media*, **32**, 1694–1712, 2020.
25. A. BERGAMINI, M. MINIACI, T. DELPERO, D. TALLARICO, B. VAN DAMME, G. HANNEMA, I. LEIBACHER, A. ZEMP, *Tacticity in chiral phononic crystals*, *Nature Communications*, **10**, 4525, 2019.
26. T.J. HEALEY, *Material symmetry and chirality in nonlinearly elastic rods*, *Mathematics and Mechanics of Solids*, **7**, 405–420, 2002.
27. J. SÁNCHEZ-DEHESA, V.M. GARCIA-CHOCANO, D. TORRENT, F. CERVERA, S. CABRERA, F. SIMON, *Noise control by sonic crystal barriers made of recycled materials*, *Journal of the Acoustical Society of America*, **129**, 1173–1183, 2011.
28. M.J. FRAZIER, *Dissipative Wave Propagation in Phononic Crystals and Metamaterials: Models and Analysis*, University of Colorado, Boulder, 2015.
29. D. RAABE, C. SACHS, P. ROMANO, *The crustacean exoskeleton as an example of a structurally and mechanically graded biological nanocomposite material*, *Acta Materialia*, **53**, 4281–4292, 2005.
30. C. LI, S. ZHANG, L. GAO, W. HUANG, Z. LIU, *Vibration attenuation investigations on a distributed phononic crystals beam for rubber concrete structures*, *Mathematical Problems in Engineering*, **2021**, 9982376, 2021.
31. S.K. YANG, S.Y. HSIA, *Reflection and transmission of the longitudinal wave at an achiral-chiral boundary*, *Japanese Journal of Applied Physics*, **36**, 1201–1208, 1997.

Received July 28, 2023; revised version September 18, 2023.

Published online October 19, 2023.
